Original Article

JCBFM

Journal of Cerebral Blood Flow & Metabolism
2021, Vol. 41(3) 530–545

DOI: 10.1177/0271678X20916860
journals.sagepub.com/home/jcbfm
SAGE

Rbfox-1 contributes to CaMKIIα expression and intracerebral hemorrhage-induced secondary brain injury via blocking micro-RNA-124

Fang Shen[1,2,*], Xiang Xu[1,*], Zhengquan Yu[1], Haiying Li[1], Haitao Shen[1], Xiang Li[1], Meifen Shen[1,2] and Gang Chen[1]

Abstract

RNA-binding protein fox-1 homolog 1 (Rbfox-1), an RNA-binding protein in neurons, is thought to be associated with many neurological diseases. To date, the mechanism on which Rbfox-1 worsens secondary cell death in ICH remains poorly understood. In this study, we aimed to explore the role of Rbfox-1 in intracerebral hemorrhage (ICH)-induced secondary brain injury (SBI) and to identify its underlying mechanisms. We found that the expression of Rbfox-1 in neurons was significantly increased after ICH, which was accompanied by increases in the binding of Rbfox-1 to Ca^{2+}/calmodulin-dependent protein kinase II (CaMKIIα) mRNA and the protein level of CaMKIIα. In addition, when exposed to exogenous upregulation or downregulation of Rbfox-1, the protein level of CaMKIIα showed a concomitant trend in brain tissue, which further suggested that CaMKIIα is a downstream-target protein of Rbfox-1. The upregulation of both proteins caused intracellular-Ca^{2+} overload and neuronal degeneration, which exacerbated brain damage. Furthermore, we found that Rbfox-1 promoted the expression of CaMKIIα via blocking the binding of micro-RNA-124 to CaMKIIα mRNA. Thus, Rbfox-1 is expected to be a promising therapeutic target for SBI after ICH.

Keywords

Rbfox-1, CaMKIIα, micro-RNA-124, intracerebral hemorrhage, secondary brain injury

Received 28 May 2019; Revised 16 January 2020; Accepted 18 January 2020

Introduction

Stroke is an important neurological disease that threatens the safety of human life, and it is also a major cause of disability and death.[1] Intracerebral hemorrhage (ICH) is a major type of stroke that accounts for approximately 10–15% of all cases.[2,3] Additionally, ICH patients have a greater degree of health loss and mortality compared with that of individuals suffering from ischemic stroke. It has been reported that approximately between 25% and 50% of patients die within one month after ICH, and only 20% of patients can recover their function within six months. Therefore, timely, safe, and effective treatment after ICH is necessary. Although much research and exploration been carried out, current treatment methods are still not ideal.

Ca^{2+}/calmodulin-dependent protein kinase II (CaMKII) is one of the most abundant protein kinases and is widely distributed throughout the body.[4] CaMKII expressed in neurons plays a role in a number of regulatory functions, such as the synthesis

[1]Department of Neurosurgery & Brain and Nerve Research Laboratory, The First Affiliated Hospital of Soochow University, Suzhou, China
[2]School of Nursing, Medical College of Soochow University, Suzhou, China

*These authors contributed equally to this work.

Corresponding authors:
Gang Chen, Department of Neurosurgery & Brain and Nerve Research Laboratory, The First Affiliated Hospital of Soochow University, 188 Shizi Street, Suzhou 215006, China.
Email: nju_neurosurgery@163.com
Meifen Shen, Department of Neurosurgery & Brain and Nerve Research Laboratory, The First Affiliated Hospital of Soochow University, 188 Shizi Street, Suzhou 215006, China.
Email: smf8165@163.com

and release of neurotransmitters, activation of ion channels, and plasticity of synapses.[5] In mammals, CaMKII is divided into the following four subtypes: α, β, γ, and δ, and CaMKIIα is almost exclusively expressed in brain.[6–8] A large number of studies have shown that CaMKIIα is involved in and mediates neuronal death in cerebral ischemia and poisoning (fluorosis), which leads to damage of the nervous system.[9–12]

Previous study has found that the expression of CaMKIIα is regulated by the RNA-binding protein, fox-1 homolog 1 (Rbfox-1).[13] Rbfox-1, a member of the Rbfox family, is conserved in human, rat, mouse, chicken, zebrafish, and frog. Mammals express three Rbfox paralogs: Rbfox-1, Rbfox-2 (RNA-binding protein, fox-1 homolog 2), and Rbfox-3 (RNA-binding protein, fox-1 homolog 3).[14] Rbfox-1 is expressed in neurons, heart, and muscle; Rbfox2 is expressed in these three tissues, as well as in stem cells, hematopoietic cells, and other cells; Rbfox-3 (also known as NeuN) is expressed only in neurons.[15] Rbfox-1 has two types: nuclear and cytoplasmic isoforms, referred to as Rbfox-1_N and Rbfox-1_C. Rbfox-1_N plays major regulatory roles in pre-mRNA alternative splicing, while Rbfox-1_C is mainly combined with the cytoplasmic target mRNA to regulate its stability and translation.[16,17] However, it is not known whether Rbfox-1 can target and regulate the expression of CaMKIIα to cause neuronal death after ICH.

In addition to Rbfox-1, CaMKIIα can also be regulated by micro-RNAs (miRNAs). MiRNAs are a class of highly conserved small, endogenous, noncoding-RNA molecules. As important post-regulators of several biological processes, miRNAs exhibit an opposite activity to that of RNA-binding proteins (RBPs) that bind complementary-target mRNAs and repress their expression.[18] Micro-RNA-124 (miR-124) has been reported to be abundantly expressed in neuronal cells.[19] In particular, CaMKIIα mRNA also contains the target sites for miR-124 binding.[13] Thus, miR-124 may compete with Rbfox-1 to regulate CaMKIIα mRNA stability and translation.

These findings suggest that targeting Rbfox-1 may provide a new way into the suppression of the adverse reactions of CaMKIIα in neuropathological events. However, the relationship and role of among Rbfox-1, CaMKIIα, and miR-124 in ICH remain obscure. Therefore, one of the purposes of the present study was to elucidate the roles and potential mechanisms of Rbfox-1 and CaMKIIα in ICH in rats. Moreover, we aimed to examine the competition between Rbfox-1 and miR-124 for CaMKIIα expression and ICH-induced brain injury and to provide a new direction for the treatment of ICH.

Materials and methods

Animals

All experiments were approved by the Ethics Committee of the First Affiliated Hospital of Soochow University and were conducted in strict accordance according to the guidelines of the National Institutes of Health on the care and use of animals. All efforts were made to minimize animal suffering and the number of animals used. ARRIVE (Animal Research: Reporting in vivo Experiments) guidelines were followed for reporting results of animal experiments. Adult male Sprague–Dawley (SD) rats (300–350 g) were purchased from the Animal Center of Chinese Academy of Sciences (Shanghai, China). They were housed in a suitable environment with a constant temperature of 23°C and relative humidity of 40% and were maintained on a 12-h light/dark cycle with unlimited access to food and water. Additionally, we controlled for the amount of animal use as much as possible and alleviated their pain during the operation.

Establishment of the experimental ICH model in rats

An experimental ICH model in vivo was established by injection of autologous blood.[2] First, SD rats were anesthetized by intraperitoneal injection of 4% chloral hydrate (10 ml/kg) and were then fixed in a prone position on the stereotaxic frame (Zhenghua Biological Equipment Co. Ltd, Anhui, China). The median scalp was shaved and sterilized, and a median incision was made to expose the periosteum. The periosteum was removed with a bone stripper to expose the anterior and sagittal sutures. A round hole corresponding to the right basal ganglia (3.5 mm to the right and 0.2-mm posterior to bregma) was drilled. Then, 100 µl of non-heparinized autologous-arterial blood collected from the heart was slowly injected (20 µl/min) into the basal ganglia through a microinjector (5.5 mm in depth). After the injection was completed, the microinjector was slowly pulled out after maintaining it in place for 5 min, and then the scalp was sutured. A schematic representation of the coronal brain sections is shown in Figure 1(a).

Experimental design

This experiment was divided into three parts. In experiment 1 (Figure 1(b)), 55 rats were randomly assigned to seven groups (Stat Trek's Random Number Generator was used. http://stattrek.com/statistics/random-number-generator.aspx), including 7 rats in the Sham group and 8 rats in each of the remaining 6 experimental groups arranged by the following times

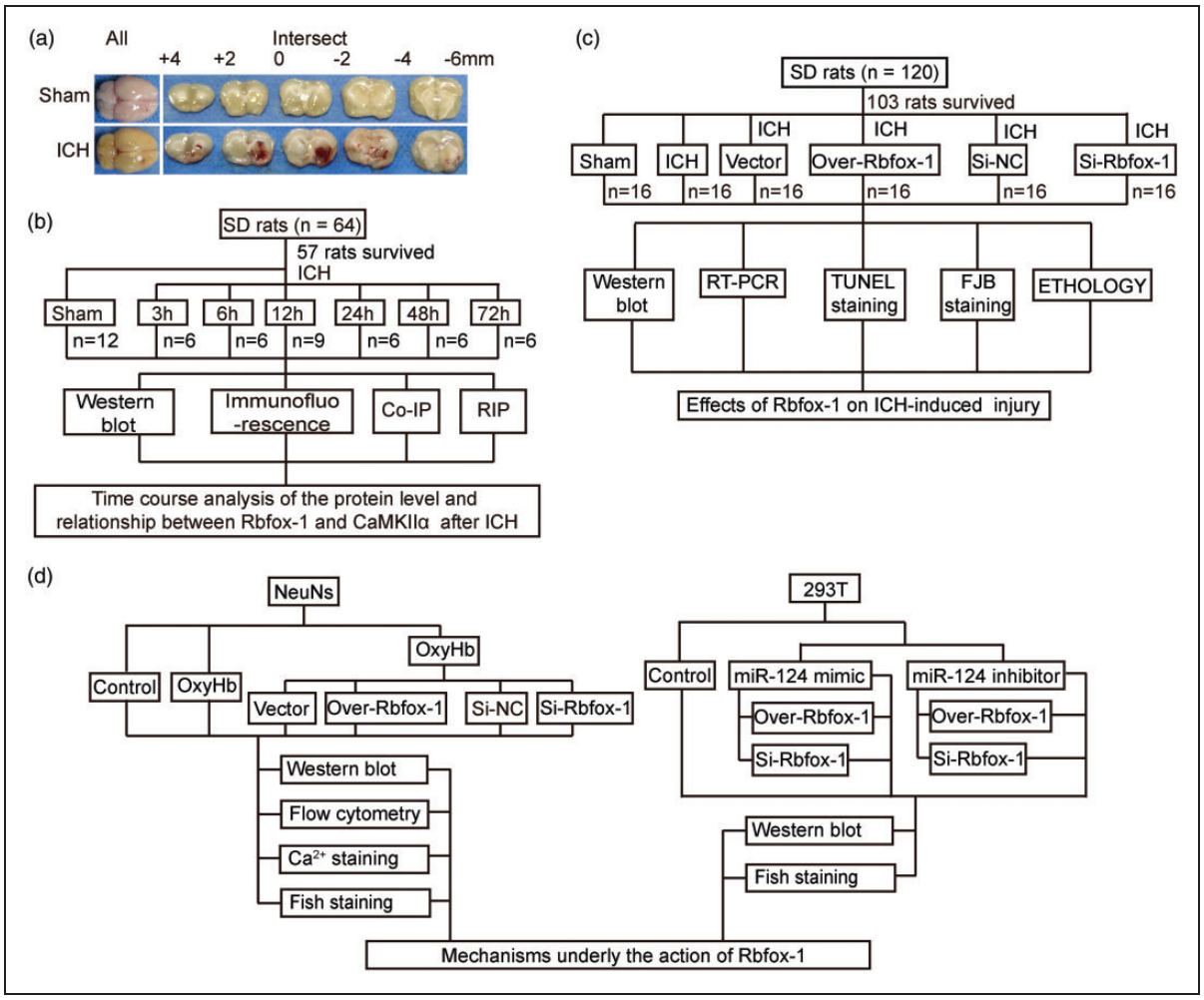

Figure 1. Intracerebral hemorrhage (ICH) model and experimental design. (a) Representative whole brains and coronal brain sections at the scheduled times after ICH. (b) Time course of the protein level and relationship between RNA-binding protein, fox-1 homolog 1 (Rbfox-1), and Ca^{2+}/calmodulin-dependent protein kinase II (CaMKIIα) after ICH in vivo. (c) The effect of Rbfox-1 on ICH-induced injury. (d) The protein levels of Rbfox-1 and CaMKIIα after ICH in vitro and the potential mechanisms.

after surgery: 3, 6, 12, 24, 48, and 72 h. When the scheduled time was reached after ICH (48 rats survived and other rats were died during the modeling of ICH, and the survive rate is 87.3%), six rats surviving in each group were randomly sacrificed, and their brain-tissue samples were obtained for subsequent time-course experiments in vivo. Additionally, the relationship between Rbfox-1 and CaMKIIα after ICH was verified by co-immunoprecipitation (Co-IP) and RNA-immunoprecipitation (RIP) testing. Since RIP testing required fresh brain tissue, we used another nine rats, including six rats in the Sham group and three rats in the ICH group.

Based on the results of experiment 1, experiment 2 exploited the time period at 12 h after ICH (Figure 1 (c)). First, 120 rats were randomly divided into the following six groups of 20 rats each (Stat Trek's Random Number Generator was used. http://stattrek.com/statistics/random-number-generator.aspx): Sham, ICH, ICH + Vector, ICH + Over-Rbfox-1, ICH + Control-siRNA, and ICH + siRNA- Rbfox-1. At 12 h after ICH (103 rats survived and other rats were died during the modeling of ICH, and the survive rate is 85.8%), six rats in each group were sacrificed, and the brain samples were extracted for Western blotting, real-time polymerase chain reaction (RT-PCR), terminal deoxynucleotidyl transferase-mediated dUTP nick-end labeling (TUNEL) staining, and fluoro-Jade B (FJB) staining. The remaining 10 rats in each group were used for ethological testing.

In experiment 3 (Figure 1(d)), primary-cultured neurons and 293 T cells were used. First, enriched neurons

were divided into the following seven groups: Control; and 1, 3, 6, 12, 24, and 48 h after exposure to oxyhemoglobin (OxyHb; 10 μM) to simulate ICH for the time-course study in vitro. Then, to explore the roles of Rbfox-1 in vitro, neurons were divided into the following six groups: Control, OxyHb, OxyHb + Vector, OxyHb + Over-Rbfox-1, OxyHb + Control-siRNA, and OxyHb + siRNA-Rbfox-1. After treatments, the cells were collected for Western blotting and flow cytometry, and the neurons were fixed with 4% paraformaldehyde for staining. Third, we explored the relationship between Rbfox-1 and miR-124. The 293 T cells were divided into seven groups and were collected for Western blotting and fluorescent staining after the corresponding interventions.

Primary neuron-enriched cultures

Primary rat cortical neurons were obtained and cultured as described previously.[20] They were isolated from the brains of fetal rats. After removing the meninges and blood vessels, the brains were digested with 0.25% trypsin for 5 min in a 37 °C environment and washed three times with phosphate-buffered saline (PBS). The digested brain tissue was filtered to take the supernatant, which was centrifuged at 1500 r/min for 5 min. Dissociated neurons were suspended in a Neurobasal-A medium containing 2% B27, 2-mM L-glutamine, 50-U/mL penicillin, and 50-U/mL streptomycin (all from Gibco, Carlsbad, CA, USA). Finally, the neurons were plated onto 6- or 12-well plates (Corning, USA) that were precoated with 0.1 mg/mL of poly-D-lysine (Sigma, USA) and were maintained at 37°C under 5% CO_2 and humidified conditions. Half of the medium was changed every two days.

Reagents

Anti-CaMKIIα antibody (ab131468), Anti-Bcl-2 antibody (ab59348), Anti-Bax antibody (ab32503), Anti-Caspase-12 antibody (ab62484), Rb mAb to NeuN (ab177487), Ms mAb to NeuN (ab104224), Anti-HA-probe antibody (ab18181), and Anti-Argonaute-2 antibody (ab186733) were from Abcam. Anti-Rbfox-1 antibody (sc-515244), normal mouse IgG (sc-2025), and Protein A/G (sc-2003) were obtained from Santa Cruz Biotechnology. β-tubulin (2128 l), Anti-Rabbit-IgG-HRP (7074 s), and Anti-Mouse-IgG-HRP (7076 s) were obtained from Cell Signaling Technology. Secondary antibodies for immunofluorescence including Alexa Fluor-488 donkey anti-rabbit IgG antibody (A21206), Alexa Fluor-488 donkey anti-mouse IgG antibody (A21202), Alexa Fluor-555 donkey anti-mouse IgG antibody (A31570), and Alexa Fluor-555 donkey anti-rabbit IgG antibody (A31572) were obtained from Life Technologies.

Transfection of the plasmid in vivo

According to the manufacturer's instructions for Entranster-in vivo DNA transfection reagent (Engreen, China), the plasmid was prepared and transferred to the rat brain. First, 5 μl of plasmid or empty vector was dissolved in 10 μl Entranster-in vivo DNA transfection reagent. After standing at room temperature for 15 min, the mixed 15 μl of the solution was injected intracerebroventricularly at 48 h before ICH.

Transfection of siRNA in vivo

The transfection of siRNA into the rat brain was performed according to the manufacturer's instructions for Entranster-in vivo RNA transfection reagent (Engreen, China). First, 500 pmol of siRNA or scramble siRNA was dissolved in 5 μl of DEPC RNase-free water, and then 10 μl of Entranster-in vivo RNA transfection reagent was added. After standing at room temperature for 15 min, the mixed 15 μl of the solution was injected intracerebroventricularly at 48 h before ICH.

The siRNA preparations came from Ribobio (RiboBio Co., Ltd, Guangzhou, China). The most effective siRNA was screened by in vitro Western blot analysis and was applied to the following experiments. Rbfox-1 siRNA sequences were as follows:

Rbfox-1 siRNA sequences:

1. Sense: GCTCGAAGGGATTTGGTTT
2. Sense: GCAATGCCTGGCTTTCCAT
3. Sense: GGTCTCGTTCTTTCTTCAT

Control-siRNA sequences:
Sense: 5′-GAGAGAAGCUGUGCUUGGUdTdT-3′
Antisense: 3′-dTdT CUCUCUUCGACACGAACCA-5′

Transfection of plasmid and siRNA in vitro

Transfection of the plasmid or siRNA into neurons was accomplished via Lipofectamine® 3000 Transfection Reagent (L3000-015, Invitrogen). After 48 h, the neurons were intervened with other reagents.

Western blot analysis

The brain was removed after lavage with PBS, and the brain tissue surrounding the hematoma was selected. The lysed brain tissue and neurons were centrifuged (12,000 r/min, 5 min, 4°C), and the supernatant was taken. The protein concentration in the sample was measured using the 96-well Cell Culture Cluster and

enhanced BCA Protein Assay Kit (Beyotime, China). The protein samples were loaded on SDS-polyacrylamide gels and were then separated and electrophoretically transferred to polyvinylidene-difluoride membranes (IPVH00010; Millipore Corporation, Billerica, MA, USA). The membrane was blocked with 5% non-fat milk at room temperature. After 1 h, the membrane was incubated overnight at 4°C with primary antibodies against Rbfox-1, CaMKIIα, caspase-12, bcl-2, and bax. Additionally, β-tubulin was used as a loading control. After three washes with PBST, the membrane was incubated in the appropriate HRP-conjugated secondary antibodies for 1.5 h at room temperature and was subsequently washed three times with PBST. Finally, the protein bands were visualized using an Enhanced Chemiluminescence (ECL) Kit (Beyotime, China) and were analyzed via the Image J Software (NIH, Bethesda, MD, USA).

Immunofluorescent analysis

The brain tissue was fixed with 4% paraformaldehyde, embedded in paraffin, and sectioned. After being heated and dewaxed, the sections were incubated overnight at 4°C with primary antibodies (diluted 1:200) and 1 h at 37°C with secondary antibodies (diluted 1:250). For cells, they could be incubated as long as they were fixed by 4% paraformaldehyde. After washing three times with PBST, the sections were sealed with DAPI Fluoromount-G@ (Southern Biotech) and coverslips (24 × 24 mm). Finally, sections were observed by a fluorescent microscope (OLYMPUS BX50/BX-FLA/DP70; Olympus Co., Japan).

Co-IP

The brain tissue was ground in lysis buffer and centrifuged to remove the supernatant. The protein A/G beads were then added to the supernatant and rotated for 1 h at 4°C. Subsequently, the samples were centrifuged, and the supernatant was taken. Specific antibodies or negative controls (e.g. normal IgG) were then added to the supernatant and rotated overnight at 4°C. Then, the beads were added again and rotated for 4 h at 4°C. After centrifugation, the precipitate was taken and washed three times. After mixing the precipitate and loading buffer, the protein was further separated and detected by SDS-PAGE and immunoblotting.

RT-PCR

The specific protocol used has been described previously.[21] In short, the protocol was divided into two steps. In the first step, the RNA was reverse transcribed into complementary DNA (cDNA) by the specific kits (RR036A, TaKaRa, Japan). In the second step, RT-PCR was performed by using other specific kits (RR420Q, TaKaRa, Japan). β-actin served as loading controls.

RIP test

The test was divided into two parts. In the first part, the target RNA was eluted through the Magna's RIP kit (17-700, Merck, Germany). The second part consisted of RT-PCR, and the specific operation steps were as completed as described above.

TUNEL staining

TUNEL staining was used to detect dead cells in brain tissue. The brain tissue was fixed with 4% paraformaldehyde, embedded in paraffin, sectioned, heated, and dewaxed. Then, the sections were perforated with 0.1% Triton X-100 for 8 min and washed three times with PBST. The TUNEL-reaction mixture was configured according to the manufacturer's protocol (DeadEnd Flurometric kit, Promega, WI, USA) and was added dropwise to the sample and incubated in a 37°C dark room for 60 min. After washing three times with PBST, the sections were sealed with DAPI Fluoromount-G@ (Southern Biotech, USA) and coverslips (24 × 24 mm). Finally, sections were observed by a fluorescent microscope (OLYMPUS BX50/BX-FLA/DP70; Olympus Co., Japan). To evaluate the extent of neuronal death, six microscopic fields per sample were examined and photographed, and the apoptotic index was defined as the average percentage of TUNEL-positive cells in each section. The count of positive cells was statistically analyzed by an observer blinded to grouping.

FJB staining

FJB staining was used to detect degenerated cells in brain tissue. The first step was the same as that for TUNEL staining. Then, the brain sections were incubated in 80% alcohol with 20% sodium hydroxide for 5 min, 70% alcohol for 2 min, distilled water for 2 min, 0.06% K permanganate for 10 min, 0.0004% FJB-working solution for 20 min and were then dried in an incubator (50–60°C) for 15–30 min. Next, the sections were placed in xylene for 2 min and were sealed with neutral gum and coverslips (24 × 24 mm). Finally, sections were observed by a fluorescent microscope (OLYMPUS BX50/BX-FLA/DP70; Olympus Co., Japan). Similarly, the count was done by an observer blinded to grouping.

Neurobehavioral scores

At the third day after ICH, rats were examined for behavioral impairments using a previously published scoring system.[22] This testing was performed by an observer who was blind to the experimental groups.

Adhesive-removal test

According to our previous report, the adhesive-removal test (also referred to as the sticky-tape test) was used to measure motor coordination and sensory neglect after ICH.[23,24] First, the rat was placed in a transparent glass-test box for a period of time, and then a 9-mm circular sticker was attached to the palm of each forepaw. The time taken to remove all stickers was recorded. Before ICH, all rats were trained for three days to ensure that the rat could remove the sticker. The day before the injury, the time to remove stickers was recorded as the baseline level. The test was then performed on days 1, 3, 7, and 14 after ICH. The recording of the data was completed by two blind researchers.

Rotarod test

The test was mainly used to assess locomotor impairments. Briefly, the rats were placed on the rotarod cylinder (ZH-300B, Anhui Zhenghua Biological Equipment Co. Ltd., Anhui, China), and the time animals remained was recorded. The speed rose at a constant rate from 4 to 30 r/min within 1 min. If the rat dropped or gripped the device and spun around for two consecutive revolutions, the experiment ended. Before modeling, all rats were trained for three days, three times a day. The day before the ICH, the average time in the test was recorded as the baseline level. The test was then performed on days 1, 3, 7, and 14 after ICH. The method of data recording was the same as adhesive-removal test.

Fluorescence in situ hybridization (Fish) staining

This detection was performed according to the manufacturer's instructions for the Fluorescent in Situ Hybridization Kit (RiboBio, China). First, the cell slides were fixed with 4% paraformaldehyde for 10 min and washed three times with PBS. One milliliter of precooled PBS with 0.5% Triton X-100 was added into each well at 4°C for 5 min. After washing three times with PBS, the cells were blocked with 200 µl of prehybridization solution (Blocking Solution: Pre-hybridization Buffer = 1:99) at 37°C for 30 min. Next, the cells were incubated overnight at 37°C with probe hybridization. After washing with cleaning fluid, the cells were incubated overnight at 4°C with primary antibodies (diluted 1:200) and for 1 h at 37 °C with secondary antibodies (diluted 1:250). After being sealed with DAPI, the cells were observed by a fluorescent microscope (OLYMPUS BX50/BX-FLA/DP70; Olympus Co., Japan) and a laser scanning confocal microscope (ZEISS LSM 880, Carl Zeiss AG, Germany).

Ca^{2+} staining

According to the manufacturer's instructions, the neurons were incubated in a calcium-ion fluorescent probe at 5 µM of Fluo-3AM (Beyotime, China) at 37°C for 30 min. Then, the cell slides were washed three times with PBS and were fixed with 4% paraformaldehyde for 20 min. Finally, the cells were observed by a fluorescent microscope (OLYMPUS BX50/BX-FLA/DP70; Olympus Co., Japan).

Annexin V and PI staining in vitro

After the intervention, the cells were trypsinized with 0.25% trypsin (without EDTA) and washed three times with PBS. After centrifugation (2000 r/min, 5 min), the cell pellet was taken and resuspended in 500-µl binding buffer. Then, 5 µl-Hoechst and 5-µl PI (KGA105, KeyGEN, China) were added to the cell medium after 15 min of incubation at room temperature in the dark. Finally, the test was performed by flow cytometry within 1 h.

Statistical analysis

GraphPad Prism 7.0 software (GraphPad, San Diego, CA, USA) was used for statistical analysis. Neurobehavioral scoring is presented as the median with the interquartile range and the Mann–Whitney U test was used to compare scores among groups. All other data were reported as the mean ± SD. One-way or two-way ANOVA was used to determine the differences between groups, and Tukey's post hoc test was used to determine the differences between two pairs in multiple groups. The correlation between two variables was assessed using Pearson's correlation test. $P < 0.05$ was considered statistically significant.

Results

ICH increases the protein levels of Rbfox-1 and CaMKIIα while also increasing the binding of Rbfox-1 to CaMKIIα mRNA

First, the ICH models of the SD rats were successfully established (Figure 1(a)). Then, the protein levels of Rbfox-1 in rat brain tissues were analyzed by Western blotting and double immunofluorescence. The results of Western blotting indicated that, compared with those of the Sham group, the protein

levels of Rbfox-1 in brain tissue were significantly increased after 12 h of ICH (Figure 2(a), $P < 0.01$). Additionally, the double-immunofluorescence assay further confirmed the ICH-induced increase in the protein levels of Rbfox-1 in neurons (Figure 2(b)). In order to verify the relationship between Rbfox-1 and CaMKIIα, we performed the Co-IP and RIP tests. As shown in Figure 2(c), the amount of CaMKIIα mRNA combined with Rbfox-1 was significantly increased after ICH ($P < 0.01$). In addition, Western blot analysis showed that the expression of CaMKIIα also increased after ICH and reached a peak level at 12 h (Figure 2(d), $P < 0.01$).

Rbfox-1 influences the level of CaMKIIα mRNA and its translation

To further verify the role of Rbfox-1 in regulating CaMKIIα, we overexpressed and knocked down Rbfox-1 by plasmid and siRNA transfection, respectively. First, the highest transfection efficiency (siRNA 1) among all the three siRNAs was analyzed by Western blotting and was used in the subsequent experiments (Figure 3(a)). Then, the transfection efficiency of the overexpression and knockdown of Rbfox-1 in brain tissue was verified by Western blot analysis (Figure 3(b), $P < 0.05$, $P < 0.01$). With the overexpression or knockdown of Rbfox-1, the content of CaMKIIα mRNA also showed a concomitant trend (Figure 3(c), $P < 0.05$, $P < 0.01$), and the expression of protein CaMKIIα in brain tissue was also increased or decreased (Figure 3(d), $P < 0.05$, $P < 0.01$).

Upregulation of Rbfox-1 promotes ICH-induced behavioral and cognitive dysfunction of rats

To identify the effects of Rbfox-1 on neurological function, we performed behavioral scoring on all rats. As shown in Figure 3(e), compared with that of the Sham group, rats after ICH showed severe neurological

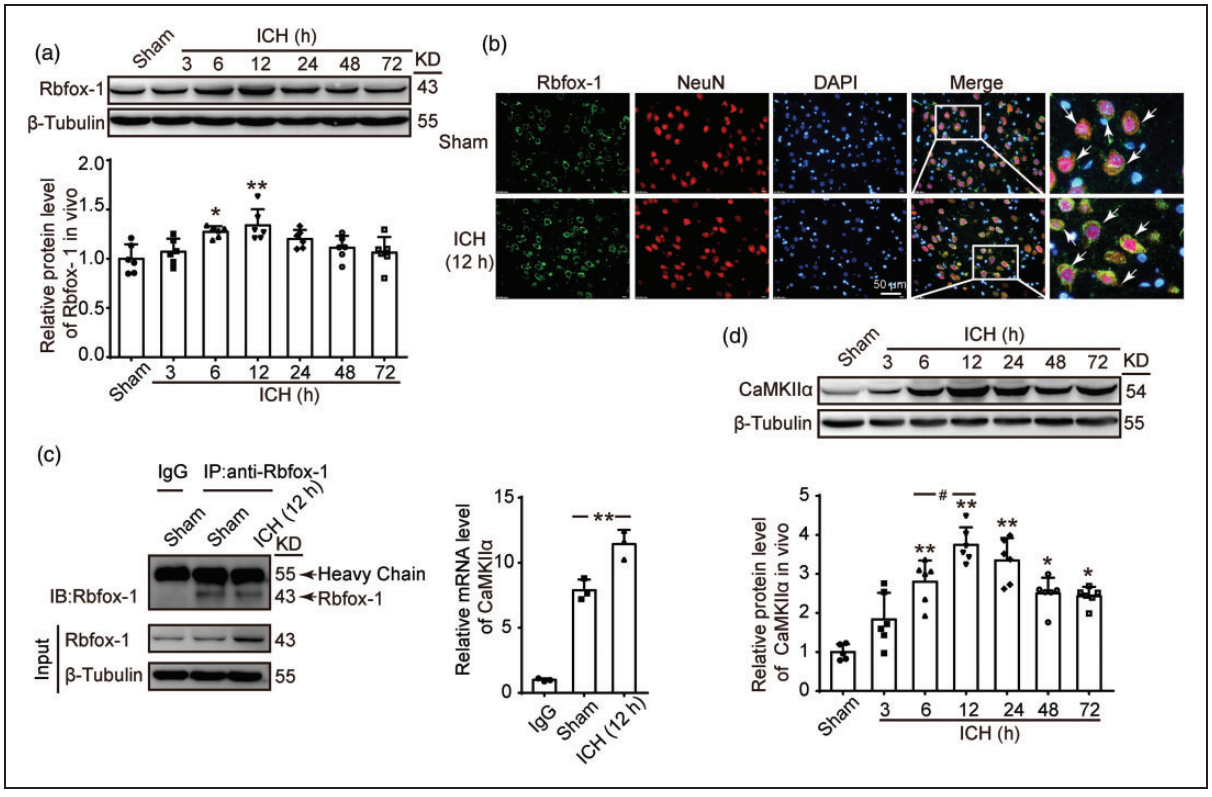

Figure 2. The protein levels of Rbfox-1 and CaMKIIα and the mRNA level of CaMKIIα in brain tissues after ICH. (a) Western blot analysis and quantification of the time course of the protein levels of Rbfox-1 in brain tissue around hematoma, $n = 6$. (b) Double-immunofluorescence analysis was performed with Rbfox-1 antibodies (green) and a neuronal marker (NeuN, red) in sections. Additionally, nuclei were fluorescently labeled with 4′-6-diamidino-2-phenylindole (DAPI) (blue). Representative images of the Sham and ICH (12 h) groups are shown. Arrows pointed to Rbfox-1-positive neurons. Scale bar = 50 μm. (c) Co-immunoprecipitation (Co-IP) and RNA Immunoprecipitation (RIP) test analysis of the interaction between Rbfox-1 and CaMKIIα mRNA in brain tissues of rats at 12 h after ICH, $n = 3$. (d) Western blot analysis and quantification of the time course of the protein levels of CaMKIIα in brain tissue around hematoma, $n = 6$. In (a, d), mean values for the Sham group were normalized to 1.0. All data are mean ± standard deviations (SD). $^{*}P < 0.05$, $^{**}P < 0.01$ vs. Sham; $^{\#}P < 0.05$ vs. 6 h.

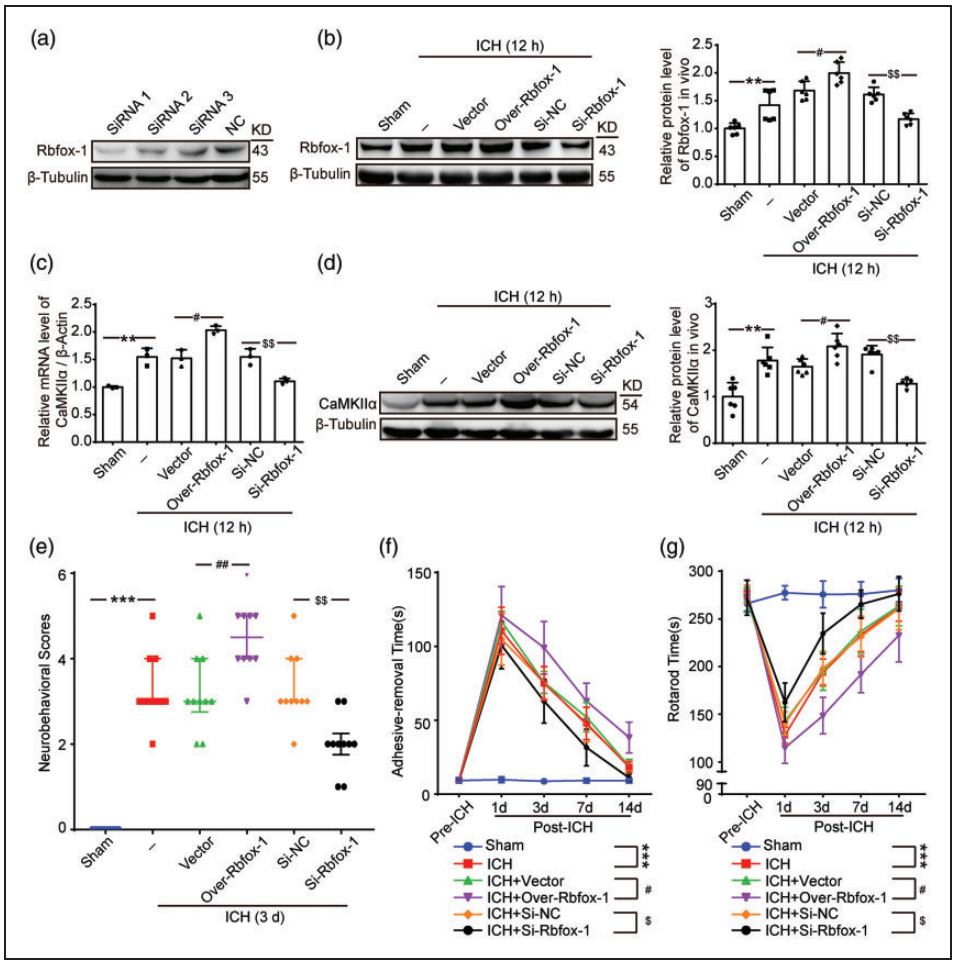

Figure 3. The effects of overexpression and knockdown of Rbfox-1 on the Rbfox-1, CaMKIIα mRNA, and CaMKIIα levels in brain tissues, and neurological function of rats after ICH. (a) The most effective siRNA was screened by 293 T cells. (b) Western blot analysis and quantification of the effects of plasmid and siRNA of Rbfox-1, $n = 6$. (c) The mRNA levels of CaMKIIα in brain tissue after overexpression and knockdown of Rbfox-1 were analyzed by polymerase chain reaction (PCR), $n = 3$. (d) Western blot analysis and quantification of the effects of overexpression and knockdown of Rbfox-1 on the protein levels of CaMKIIα in brain tissue, $n = 6$. (e) Neurobehavioral scores. (f) Adhesive-removal test. (g) Rotarod test. In (b–d), mean values for the Sham group were normalized to 1.0, data are mean ± SD. $^{**}P < 0.01$ vs. Sham; $^{\#}P < 0.05$ vs. ICH + Vector; $^{\$\$}P < 0.01$vs. ICH + Si-NC. In (e), the data are median and interquartile range; in (f, g), data are mean ± SD. $^{***}P < 0.001$ vs. Sham, $^{\#}P < 0.05$, $^{\#\#}P < 0.01$ vs. ICH + Vector, $^{\$}P < 0.05$, $^{\$\$}P < 0.01$ vs. ICH + Si-NC, $n = 10$.

impairment ($P < 0.001$), and upregulation of Rbfox-1 significantly exacerbated the degree of damage and delayed its recovery ($P < 0.01$). Conversely, the decrease in Rbfox-1 significantly reduced neurological damage (Figure 3(e), $P < 0.01$). Aside from the behavioral score, the functional improvements associated with Rbfox-1 were also corroborated by assessments with the adhesive-removal and rotarod tests. In adhesive-removal test, knockdown of Rbfox-1 resulted in significant recovery of somatosensory function following ICH (Figure 3(f), $P < 0.05$). In addition, in the rotarod test, rats that had down-regulated Rbfox-1 expression were able to remain longer on the accelerating beam compared to that of vehicle rats after ICH (Figure 3(g), $P < 0.05$).

Upregulation of Rbfox-1 exacerbates ICH-induced neuronal injury in brain tissues of rats

To further assess the effects of Rbfox-1 on neurons, TUNEL and FJB staining were performed to assess neuronal death and degeneration in the brain at 12 h after ICH. Compared with that of the Sham group, the index of TUNEL positive neurons was significantly increased, the phenomenon of which was reversed after downregulating Rbfox-1 (Figure 4(a) and (b), $P < 0.001$, $P < 0.01$). A significant positive correlation existed between CaMKIIα levels and percentage of TUNEL positive neurons in brain tissues within 12 h after ICH (Figure 4(c), $P < 0.001$). Consistently, the number of FJB positive cells both in the cortex and

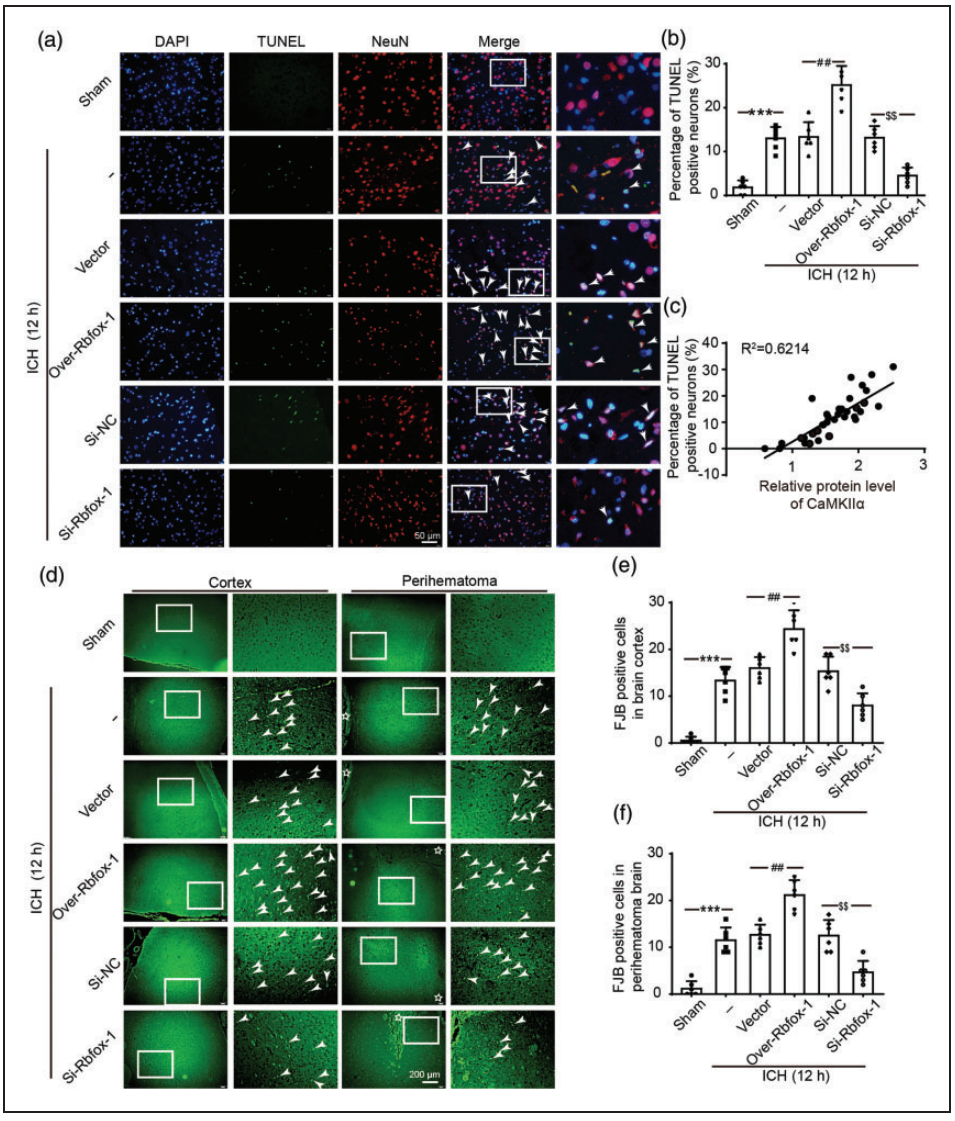

Figure 4. The effects of overexpression and knockdown of Rbfox-1 on neuronal death and degeneration in brain tissues. (a) Double staining for terminal deoxynucleotidyl transferase-mediated dUTP nick end labeling (TUNEL) (green) neuronal marker (NeuN, red). Nuclei were fluorescently labeled DAPI (blue). Arrows point to TUNEL-positive cells, Scale bar = 50 μm. The percentage of TUNEL-positive cells is shown (b). (c) Pearson correlation coefficient between CaMKIIα levels with percentage of TUNEL-positive neurons in brain tissues within 12 h after ICH. R^2=0.6214, $P < 0.001$, $n = 36$. (d) Positive fluoro-Jade B (FJB) staining and arrows point to FJB-positive cells. Scale bar = 200 μm. Counts of FJB-positive cells in brain cortex and perihematoma brain are shown (e, f). In (b, e, f), data are mean ± SD, $^{***}P < 0.001$ vs. Sham; $^{\#\#}P < 0.01$ vs. ICH + Vector; $^{\$\$}P < 0.01$ vs. ICH + Si-NC, $n = 6$.

the perihematoma brain showed the same trend as the number of TUNEL-positive cells (Figure 4(d) to (f), $P < 0.001$, $P < 0.01$).

ICH increases the protein levels of Rbfox-1 and CaMKIIα in cultured neurons

To further clarify the expression of Rbfox-1 and CaMKIIα after ICH, we established an in vitro model using cultured neurons and OxyHb. Similar to in vivo data, the trend of the protein levels of Rbfox-1 and CaMKIIα in cultured neurons was increased after exposure to OxyHb. Western blot analysis showed that the expressions of Rbfox-1 and CaMKIIα were significantly increased at 6 h (Figure 5(a) and (b), $P < 0.01$). We also confirmed the transfection efficiency of siRNA and plasmid in cultured neurons. Similarly, the protein levels of CaMKIIα showed the same changes as those of Rbfox-1 in cultured neurons after overexpression or knockdown of Rbfox-1 (Figure 5(c) and (d), $P < 0.05$, $P < 0.01$).

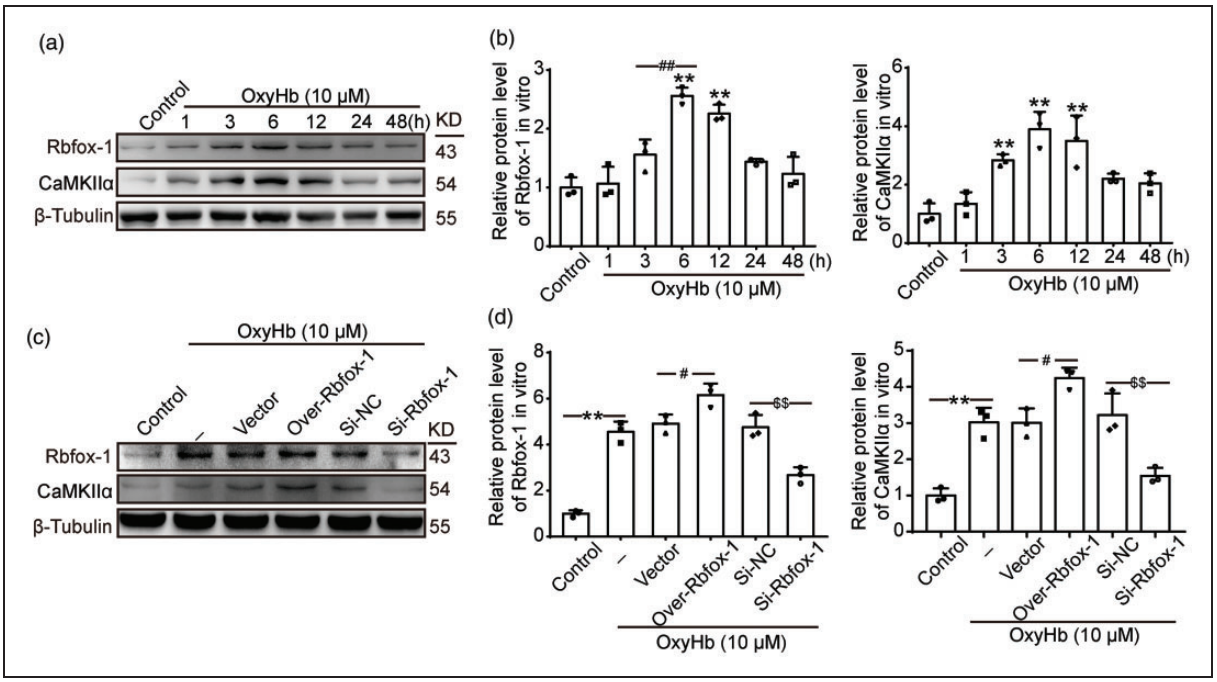

Figure 5. The protein levels of Rbfox-1 and CaMKIIα in neurons after oxyhemoglobin (OxyHb) treatment and overexpression and knockdown of Rbfox-1. (a, b) Western blot analysis and quantification of the time course of the protein levels of Rbfox-1 and CaMKIIα in cultured neurons. (c, d) Western blot analysis and quantification of the effects of overexpression and knockdown of Rbfox-1 on the protein levels of Rbfox-1and CaMKIIα in cultured neurons. In (b, d), mean values for the control group were normalized to 1.0. Data are mean ± SD. (b) $^{**}P < 0.01$ vs. Control; $^{\#\#}P < 0.01$ vs. 6 h, $n = 3$. (d) $^{**}P < 0.01$ vs. Control; $^{\#}P < 0.05$ vs. OxyHb + Vector; $^{\$\$}P < 0.01$ vs. OxyHb + Si-NC, $n = 3$.

Downregulated Rbfox-1 exerts neuroprotective effects by decreasing apoptosis and reducing Ca^{2+} overload in cultured neurons after OxyHb treatment

To ascertain the effects of Rbfox-1 on apoptosis, the protein levels of cleaved caspase-12, bax, and bcl-2 in neurons were detected by Western blot analysis (Figure 6(a) and (b)). Compared with those of the Control group, the ratio of bax/bcl-2 and the activation of caspase-12 were increased in neurons after OxyHb intervention (Figure 6(b), $P < 0.01$). Overexpression of Rbfox-1 exacerbated these behaviors, while knocking down Rbfox-1 suppressed OxyHb-induced apoptosis (Figure 6(b), $P < 0.01$). Furthermore, we performed Annexin V and PI staining in vitro to identify effects of Rbfox-1 on neuronal apoptosis (Figure 6(c) and (d)). Flow-cytometry analysis showed a high apoptotic ratio (PI+/Annexin V+ and PI−/Annexin V+ neurons) after OxyHb treatment, relative to the Control group (Figure 6(d), $P < 0.05$). When we down-regulated the levels of intracellular Rbfox-1, the apoptosis of neurons caused by OxyHb was significantly reduced (Figure 6 (d), $P < 0.05$). We also performed Ca^{2+} staining to test the intracellular Ca^{2+} levels in neurons. As shown in Figure 6(e), Ca^{2+} overload was observed in neurons exposed to OxyHb. When Rbfox-1 was inhibited, the intracellular Ca^{2+} level also decreased significantly.

Rbfox-1 competes with miR-124 to regulate CaMKIIα mRNA concentration and translation

To further confirm the binding of Rbfox-1 to target CaMKIIα mRNA, we performed co-localization using Fish and immunofluorescence staining in cultured neurons. Compared with those of the control group, the levels of Rbfox-1 and target CaMKIIα mRNA in neurons were significantly increased after OxyHb intervention (Figure 7(a)). Then, we further investigated the effects of Rbfox-1 and miR-124 interactions on the expression of CaMKIIα (Figure 7(b) and (c)). Western blotting results showed that the expression of CaMKIIα was inhibited after simple transfection of miR-124 mimics (Figure 7(c), $P < 0.05$), and this inhibition was reversed after overexpression of Rbfox-1 (Figure 7(c), $P < 0.05$). Meanwhile, simple transfection of a miR-124 inhibitor showed a similar effect as overexpression of Rbfox-1 (Figure 7(c), $P < 0.05$). After Rbfox-1 was lowered in this case, the level of CaMKIIα also dropped (Figure 7(c), $P < 0.05$). These results indicated that Rbfox-1 could competitively block the inhibition of CaMKIIα expression by miR-124. Then, we further explored the mechanism by which Rbfox-1 and miR-124 competitively regulate the expression of CaMKIIα. By Fish and immunofluorescence double staining, the expression of

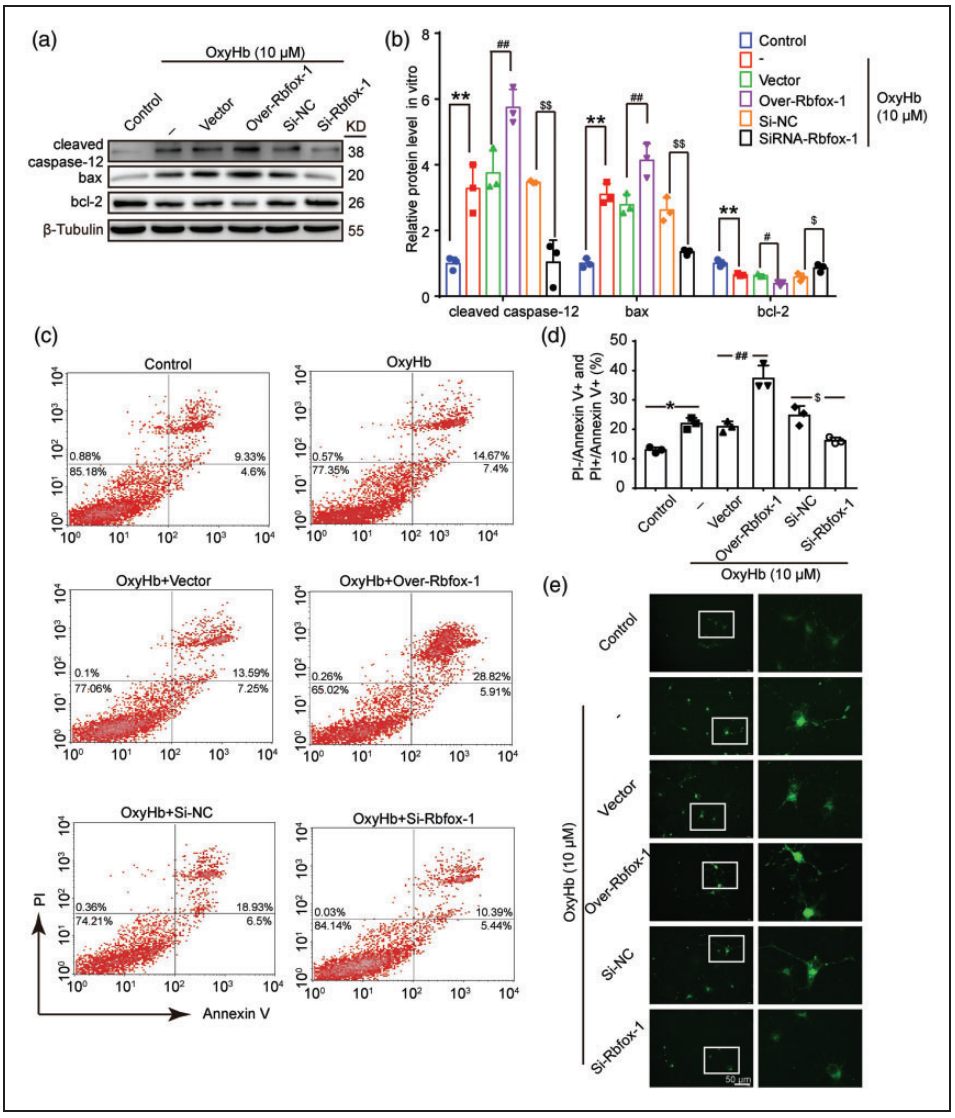

Figure 6. The effects of overexpression and knockdown of Rbfox-1 on OxyHb-induced neuronal apoptosis. (a, b) Western blot analysis and quantification of the effects of overexpression and knockdown of Rbfox-1 on the protein levels of cleaved caspase-12, bax, and bcl-2 in cultured neurons, $n = 3$. (c, d) Annexin V and PI double staining and flow-cytometry analysis showed neuronal apoptosis in various groups in vitro. PI−/Annexin V+ and PI+/Annexin V+ indicated apoptotic neurons, $n = 3$. (e) Ca^{2+} staining was used to analyze intracellular Ca^{2+} concentration in cultured neurons. Scale bar = 50 μm. All data are mean ± SD. In (b), mean values for the control group were normalized to 1.0. $^{**}P < 0.01$ vs. Control; $^{\#}P < 0.05$, $^{\#\#}P < 0.01$ vs. OxyHb + Vector; $^{\$}P < 0.05$, $^{\$\$}P < 0.01$ vs. OxyHb + Si-NC. In (d), $^{*}P < 0.05$ vs. Control; $^{\#\#}P < 0.01$ vs. OxyHb + Vector; $^{\$}P < 0.05$ vs. OxyHb + Si-NC.

Argonaute 2 (AGO2) was significantly increased after miR-124 mimic treatment, while overexpression of Rbfox-1 reversed miR-124 mimic-mediated overexpression of AGO2 (Figure 7(d)).

Discussion

As a common type of stroke, ICH often leads to disability and death of patients. An increasing amount of attention and research has been obtained in hopes of finding effective targets for the treatment of ICH and ICH-induced SBI.

Recently, Rbfox-1 has been extensively studied in various diseases, such as myotonic dystrophy and diabetes.[25,26] In addition, abnormal expression of Rbfox-1 may cause neurological disorders, so it has been regarded as a hotspot for neurological diseases. Vuong et al.[27] found that the loss of Rbfox-1 in mice led to excessive excitation of neurons and induced epileptic seizures. Many studies have also found that the Rbfox-1 gene is closely related to Alzheimer's

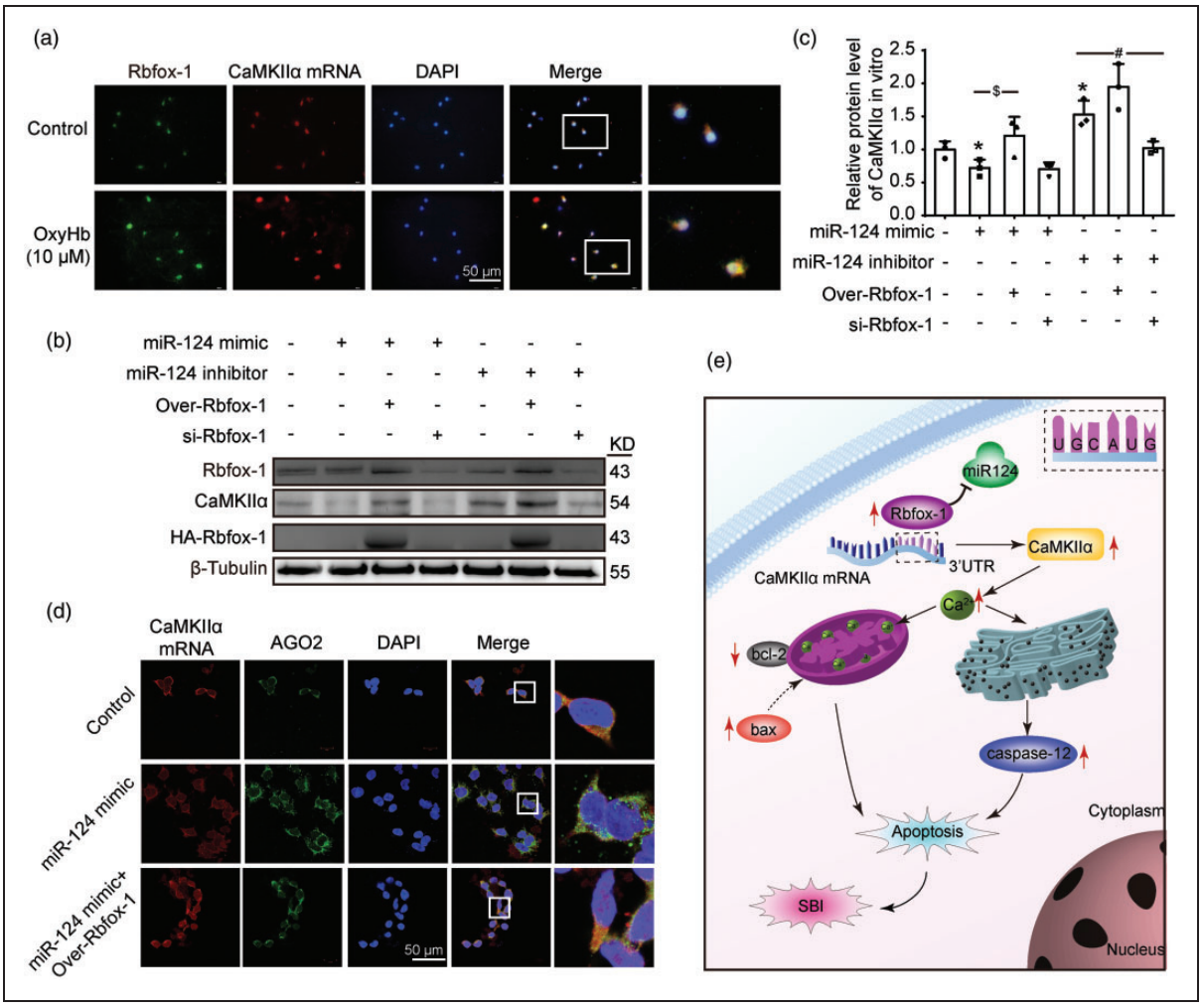

Figure 7. The roles of micro-RNA-124 (miR-124) with Rbfox-1 and CaMKIIα, and the roles of Rbfox-1 in SBI after ICH. (a) The co-localization of Rbfox-1 and CaMKIIα mRNA in cultured neurons after OxyHb treatment. Double staining for CaMKIIα mRNA (red) by Fish and Rbfox-1 (green) by immunofluorescence. And nuclei were fluorescently labeled with DAPI (blue). Scale bar = 50 μm. (b, c) The competition of Rbfox-1 and miR-124 on CaMKIIα expression. 293 T cells were co-transfected with miR-124 mimics or miR-124 inhibitors with or without over-Rbfox-1 or si-Rbfox-1 for 48 h. Western-blot analysis and quantification of the protein levels of Rbfox-1 and CaMKIIα in 293 T cells, $n = 3$. In (c), mean values for the control group were normalized to 1.0. Data are mean ± SD. $^{*}P < 0.05$ vs. Control group; $^{\$}P < 0.05$ vs. miR-124 mimic group; $^{\#}P < 0.05$ vs. miR-124 inhibitor group. (d) Double staining for CaMKIIα mRNA (red) by FISH and Argonaute2 (AGO2) (green) in 293 T cells by immunofluorescence. Scale bar = 50 μm. (e) The mechanism of Rbfox-1 in SBI after ICH. After ICH, Rbfox-1 could compete with miR-124 for CaMKIIα mRNA to stabilize the CaMKIIα mRNA, and promote CaMKIIα mRNA expression, which in turn leaded to overload of Ca^{2+} and activated the apoptosis program.

disease (AD). Alkallas et al.[28] found that the reduction of Rbfox-1 affected proteins that encode synaptic transmission, leading to synaptic impairment. However, there has been no research to exam the link between Rbfox-1 and ICH. In the present study, we focused on the expression of Rbfox-1 in rat brain tissues after ICH and investigated its possible functions following ICH. Our study found that the expression of Rbfox-1 increased after ICH.

As a class of RBPs, the main functions of Rbfox-1 are to regulate the stability and translation of target mRNAs and to control the expression of downstream proteins.[13,29,30] Rbfox-1 has a highly conserved RNA recognition motif (RRM),[31,32] which binds to the (U) GCAUG motif with high affinity and specificity.[15] In most cases, whether in AD or epilepsy, Rbfox-1 abnormality is not the direct cause of disease status but is due to the imbalance of the downstream target proteins caused by the abnormality of Rbfox-1. For example, a downregulation of Rbfox-1 led to a decrease in Vamp1 in inhibitory neurons, resulting in increased excitability of the neurons.[27]

In addition to the above protein, CaMKIIα is one of the downstream-target proteins of Rbfox-1,[13] for which

our present study further verified. After ICH, the combination of Rbfox-1 and CaMKIIα mRNA was increased, which upregulated the stability and translation of mRNA. On the basis of ICH, we also upregulated or knocked down intracellular Rbfox-1 to observe the condition of CaMKIIα. When Rbfox-1 was knocked down or upregulated, the concentration and translation level of CaMKIIα mRNA exhibited a concomitant trend. The above data confirmed that CaMKIIα was the target protein of Rbfox-1 after ICH.

Previous studies have found that excessive CaMKIIα is associated with a variety of symptoms, including aggravating hepatic ischemia–reperfusion (I/R) damage[10] and participating in the induction of apoptosis in bone cells[33] and neurons.[9] We also found that the overexpression of Rbfox-1 and CaMKIIα was closely related to neuronal death and degeneration, as well as to neurological damage following ICH.

As the major isoform of CaMKII, CaMKIIα is highly sensitive to intracellular Ca^{2+} levels.[11,12] Intracellular Ca^{2+} plays a pivotal role in multiple physiological processes and in responding to noxious stimulation and is closely related to cell apoptosis and necrosis.[34,35] In normal physiological conditions, the concentration of Ca^{2+} in the extracellular matrix is much higher than the cytoplasmic-free Ca^{2+} concentration. In the early stage after ICH, Ca^{2+} channel receptors on the cell membrane are activated, resulting in a massive influx of Ca^{2+} and a calcium overload in neurons.[36,37] Our results showed that the intracellular Ca^{2+} concentration was significantly further increased after up-regulation of Rbfox-1, and inhibition of its expression reversed the increase in Ca^{2+} concentration induced by ICH. Sustained intracellular Ca^{2+} elevation activates endoplasmic-reticulum (ER) stress.[36] Additionally, caspase-12 is significantly expressed after up-regulation of Rbfox-1. Beyond this, Ca^{2+} may also cause mitochondrial dysfunction.[38] Overexpression of Rbfox-1 could alter the expression of the bcl-2 family of proteins, resulting in a further increase in bax expression and less expression of bcl-2 in neurons after ICH.

A previous study found that, in addition to the binding motif of Rbfox-1, there are recognition sites of miR-124 at the 3′UTR of CaMKIIα mRNA.[27] Growing evidence has shown that miR-124 is involved in the pathogenesis of various diseases, and its related critical roles have been increasingly recognized. A previous study showed that gain of miR-124 function resulted in reduced neuronal apoptosis and death induced by oxygen and glucose deprivation (OGD).[39] Another study also confirmed that overexpression of miR-124 could decrease protein deubiquitination and participated in post-ischemic neuroplasticity and angiogenesis.[40] With the miR-124 site overlapping with the GCAUG motif, miR-124 may compete with Rbfox-1 to regulate CaMKIIα mRNA stability and translation after ICH. To validate this hypothesis, in the in vitro experiments of the present study, we applied miR-124 mimics and miR-124 inhibitors. After administration of miR-124 mimics, the expression of CaMKIIα was reduced, while upregulation of Rbfox-1 returned the expression of CaMKIIα to normal levels.

Studies have confirmed that miRNAs mediate post-transcriptional gene silencing by inhibiting mRNA translation or bringing about their cleavage and degradation.[41] This process occurs in the RNA-induced silencing complex (RISC), in which AGO2 is one of the central enzymes and plays an important role in gene silencing in various organisms.[42–44] Previous studies have confirmed that miR-124 inhibition resulted in an increased mRNA expression level and decreased AGO2 binding in hippocampal neurons.[45] Similarly, after giving miR-124 mimics, the level of CaMKIIα mRNA decreased, while the expression of AGO2 was significantly increased in 293 T cells. On the basis of the above findings, the levels of CaMKIIα mRNA and AGO2 were restored to normal after upregulation Rbfox-1 in the present study. Hence, the above results ultimately confirmed our hypothesis.

In addition to Rbfox-1 and miR-124, ROS are known to be strongly related to CaMKII. Several evidences have demonstrated that reactive oxygen species (ROS) play critical roles in CaMKII activation-mediated apoptosis in tumor cells, cardiomyocyte, and vascular smooth muscle cells.[46–48] ROS in nerve cells are also increased after ICH, and excessive ROS could lead to oxidative stress, destroying DNA and protein, and ultimately leading to cell apoptosis.[49] However, the relationship between ROS and CaMKIIα has not been verified in ICH models, and this may be our next research direction.

In conclusion, Rbfox-1 and miR-124 may be the therapeutic target after ICH. MiR-124 mimics have shown the therapeutic value for central nervous system (CNS) injury in experimental animal models.[50] However, the delivery methods, time windows, and dosage time of miRNA-based drugs need to be further studied. We also hope to develop new strategies to pave the way for the clinical application of Rbfox-1 and miR-124-based therapies in ICH patients.

The current study also has some limitations. First, in our experiment, we only used healthy adult male SD rats to establish the ICH model, so different genders and ages of animals should be tested in further studies. Next, we chose 12 h for the intervention point for the following investigations via the first experiment, but whether there were other more suitable times requires further exploration. In addition, we only used OxyHb

to simulate ICH in vivo, but the potential effects of many other relevant components in blood should also be considered.[51,52] Additionally, one RBP corresponds to multiple target mRNAs, and one mRNA is also regulated by multiple RBPs and miRNAs. Therefore, we will need to explore the regulation of Rbfox-1 and CaMKIIα further.

Conclusions

This study demonstrated the mechanism of Rbfox-1 in inducing neurological damage after ICH. As a class of RBPs, the expression of Rbfox-1 and its target protein CaMKIIα were significantly elevated, which led to overload of Ca2+ in neurons and activated the apoptotic program. Additionally, these induced changes also compromised the cognitive behavior of the animals. Moreover, we also found that miR-124 could compete with Rbfox-1 to inhibit CaMKIIα expression. These findings suggest that Rbfox-1 and miR-124 may be the promising therapeutic target for improving the prognosis of patients with ICH.

Funding

The author(s) disclosed receipt of the following financial support for the research, authorship, and/or publication of this article: This work was supported by the National Key R&D Program of China (No. 2018YFC1312600 & No. 2018YFC1312601), the National Natural Science Foundation of China (No. 81971106), the Project of Jiangsu Provincial Medical Innovation Team (No. CXTDA2017003), Suzhou Key Medical Centre (No. Szzx201501), Scientific Department of Jiangsu Province (No. BE2017656), and Suzhou Government (No. LCZX201601).

Declaration of conflicting interests

The author(s) declared no potential conflicts of interest with respect to the research, authorship, and/or publication of this article.

Authors' contributions

GC and MS conceived and designed the study. FS and XX performed the experiments and wrote the paper. HL assisted in the use of the laser scanning confocal microscope. HS and XL helped conduct the literature review. ZY and GC reviewed and edited the manuscript. All authors read and approved the manuscript.

Supplemental material

Supplemental material for this article is available online.

ORCID iD

Gang Chen https://orcid.org/0000-0002-0758-1907

References

1. Saand AR, Yu F, Chen J, et al. Systemic inflammation in hemorrhagic strokes – a novel neurological sign and therapeutic target? *J Cereb Blood Flow Metab* 2019; 39: 959–988.
2. Shen H, Liu C, Zhang D, et al. Role for RIP1 in mediating necroptosis in experimental intracerebral hemorrhage model both in vivo and in vitro. *Cell Death Dis* 2017; 8: e2641.
3. Lee L, Lo YT, See AAQ, et al. Long-term recovery profile of patients with severe disability or in vegetative states following severe primary intracerebral hemorrhage. *J Crit Care* 2018; 48: 269–275.
4. Zhu MX, Lu C, Xia CM, et al. Simvastatin pretreatment protects cerebrum from neuronal injury by decreasing the expressions of phosphor-CaMK II and AQP4 in ischemic stroke rats. *J Mol Neurosci* 2014; 54: 591–601.
5. Colbran RJ. Targeting of calcium/calmodulin-dependent protein kinase II. *Biochem J* 2004; 378: 1–16.
6. Wen XJ, Li XH, Li H, et al. CaMK II gamma down regulation protects dorsal root ganglion neurons from ropivacaine hydrochloride neurotoxicity. *Sci Rep* 2017; 7: 5262.
7. Ataei N, Sabzghabaee AM and Movahedian A. Calcium/calmodulin-dependent protein kinase II is a ubiquitous molecule in human long-term memory synaptic plasticity: a systematic review. *Int J Prevent Med* 2015; 6: 88.
8. Wei Y, Wang R and Teng J. Inhibition of calcium/calmodulin-dependent protein kinase iialpha suppresses oxidative stress in cerebral ischemic rats through targeting glucose 6-phosphate dehydrogenase. *Neurochem Res* 2019; 44: 1613–1620.
9. Zhan L, Lu Z, Zhu X, et al. Hypoxic preconditioning attenuates necroptotic neuronal death induced by global cerebral ischemia via Drp1-dependent signaling pathway mediated by CaMKIIalpha inactivation in adult rats. *FASEB J* 2019; 33: 1313–1329.
10. Zheng D, Li Z, Wei X, et al. Role of miR-148a in mitigating hepatic ischemia-reperfusion injury by repressing the TLR4 signaling pathway via targeting CaMKIIalpha in vivo and in vitro. *Cell Physiol Biochem* 2018; 49: 2060–2072.
11. Teng Y, Zhang J, Zhang Z, et al. The effect of chronic fluorosis on calcium ions and CaMKIIalpha, and c-fos expression in the rat hippocampus. *Biol Trace Element Res* 2018; 182: 295–302.
12. Ahmed ME, Dong Y, Lu Y, et al. Beneficial Effects of a CaMKIIalpha Inhibitor TatCN21 Peptide in Global Cerebral Ischemia. *J Mol Neurosci* 2017; 61: 42–51.
13. Lee JA, Damianov A, Lin CH, et al. Cytoplasmic rbfox1 regulates the expression of synaptic and autism-related genes. *Neuron* 2016; 89: 113–128.
14. Kuroyanagi H. Fox-1 family of RNA-binding proteins. *Cell Mol Life Sci* 2009; 66: 3895–3907.
15. Gu L, Bok D, Yu F, et al. Downregulation of splicing regulator RBFOX1 compromises visual depth perception. *PLoS One* 2018; 13: e0200417.
16. Kucherenko MM and Shcherbata HR. Stress-dependent miR-980 regulation of Rbfox1/A2bp1 promotes

ribonucleoprotein granule formation and cell survival. *Nat Commun* 2018; 9: 312.
17. Conboy JG. Developmental regulation of RNA processing by Rbfox proteins. *Wiley Interdisciplin Rev RNA* 2017; 8: e1398.
18. Michlewski G and Caceres JF. Post-transcriptional control of miRNA biogenesis. *RNA* 2019; 25: 1–16.
19. He F, Liu H, Guo J, et al. Inhibition of MicroRNA-124 reduces cardiomyocyte apoptosis following myocardial infarction via targeting STAT3. *Cell Physiol Biochem* 2018; 51: 186–200.
20. Pacifici M and Peruzzi F. Isolation and culture of rat embryonic neural cells: a quick protocol. *J Visual Exp* 2012; e3965.
21. Wang Z, Chen Z, Yang J, et al. Treatment of secondary brain injury by perturbing postsynaptic density protein-95-NMDA receptor interaction after intracerebral hemorrhage in rats. *J Cereb Blood Flow Metab* 2019; 39: 1588–1601.
22. Cao J, Zhuang Y, Zhang J, et al. Leucine-rich repeat kinase 2 aggravates secondary brain injury induced by intracerebral hemorrhage in rats by regulating the P38 MAPK/Drosha pathway. *Neurobiol Dis* 2018; 119: 53–64.
23. Chau MJ, Deveau TC, Gu X, et al. Delayed and repeated intranasal delivery of bone marrow stromal cells increases regeneration and functional recovery after ischemic stroke in mice. *BMC Neurosci* 2018; 19: 20.
24. Rewell SS, Churilov L, Sidon TK, et al. Evolution of ischemic damage and behavioural deficit over 6 months after MCAo in the rat: selecting the optimal outcomes and statistical power for multi-centre preclinical trials. *PLoS One* 2017; 12: e0171688.
25. Sellier C, Cerro-Herreros E, Blatter M, et al. rbFOX1/MBNL1 competition for CCUG RNA repeats binding contributes to myotonic dystrophy type 1/type 2 differences. *Nat Commun 2018*; 9: 2009.
26. Juan-Mateu J, Rech TH, Villate O, et al. Neuron-enriched RNA-binding proteins regulate pancreatic beta cell function and survival. *J Biol Chem* 2017; 292: 3466–3480.
27. Vuong CK, Wei W, Lee JA, et al. Rbfox1 regulates synaptic transmission through the inhibitory neuron-specific vSNARE Vamp1. *Neuron* 2018; 98: 127–141.e127.
28. Alkallas R, Fish L, Goodarzi H, et al. Inference of RNA decay rate from transcriptional profiling highlights the regulatory programs of Alzheimer's disease. *Nat Commun* 2017; 8: 909.
29. Park C, Choi S, Kim YE, et al. Stress granules contain Rbfox2 with cell cycle-related mRNAs. *Sci Rep* 2017; 7: 11211.
30. Ying Y, Wang XJ, Vuong CK, et al. Splicing activation by Rbfox requires self-aggregation through its tyrosine-rich domain. *Cell* 2017; 170: 312–323.e310.
31. Damianov A, Ying Y, Lin CH, et al. Rbfox proteins regulate splicing as part of a large multiprotein complex LASR. *Cell* 2016; 165: 606–619.
32. Weyn-Vanhentenryck SM, Feng H, Ustianenko D, et al. Precise temporal regulation of alternative splicing during neural development. *Nat Commun* 2018; 9: 2189.
33. Liu W, Xu C, Ran D, et al. CaMK mediates cadmium induced apoptosis in rat primary osteoblasts through MAPK activation and endoplasmic reticulum stress. *Toxicology* 2018; 406–407: 70–80.
34. Khaw-On P, Pompimon W and Banjerdpongchai R. Apoptosis Induction via ATM phosphorylation, cell cycle arrest, and ER stress by goniothalamin and chemodrugs combined effects on breast cancer-derived MDA-MB-231 cells. *Biomed Res Int* 2018; 2018: 7049053.
35. Pittas K, Vrachatis DA, Angelidis C, et al. The role of calcium handling mechanisms in reperfusion injury. *Curr Pharm Des* 2018; 24: 4077–4089.
36. Verma M, Wills Z and Chu CT. Excitatory dendritic mitochondrial calcium toxicity: implications for Parkinson's and other neurodegenerative diseases. *Front Neurosci* 2018; 12: 523.
37. Shen J, Tu L, Chen D, et al. TRPV4 channels stimulate Ca(2+)-induced Ca(2+) release in mouse neurons and trigger endoplasmic reticulum stress after intracerebral hemorrhage. *Brain Res Bull* 2018; 146: 143–152.
38. Stacchiotti A and Favero G. Perspective: mitochondria-ER contacts in metabolic cellular stress assessed by microscopy. *Cells* 2018; 8: 5.
39. Sun Y, Gui H, Li Q, et al. MicroRNA-124 protects neurons against apoptosis in cerebral ischemic stroke. *CNS Neurosci Ther* 2013; 19: 813–819.
40. Doeppner TR, Kaltwasser B, Sanchez-Mendoza EH, et al. Lithium-induced neuroprotection in stroke involves increased miR-124 expression, reduced RE1-silencing transcription factor abundance and decreased protein deubiquitination by GSK3beta inhibition-independent pathways. *J Cereb Blood Flow Metab* 2017; 37: 914–926.
41. Hammond SM. An overview of microRNAs. *Adv Drug Deliv Rev* 2015; 87: 3–14.
42. Azlan A, Dzaki N and Azzam G. Argonaute: the executor of small RNA function. *J Genet Genom* 2016; 43: 481–494.
43. Liu J, Carmell MA, Rivas FV, et al. Argonaute2 is the catalytic engine of mammalian RNAi. *Science* 2004; 305: 1437–1441.
44. Kutsche LK, Gysi DM, Fallmann J, et al. Combined experimental and system-level analyses reveal the complex regulatory network of miR-124 during human neurogenesis. *Cell Syst* 2018; 7: 438–452.e438.
45. Malmevik J, Petri R, Klussendorf T, et al. Identification of the miRNA targetome in hippocampal neurons using RIP-seq. *Sci reports* 2015; 5: 12609.
46. Hu J, Zhang Y, Jiang X, et al. ROS-mediated activation and mitochondrial translocation of CaMKII contributes to Drp1-dependent mitochondrial fission and apoptosis in triple-negative breast cancer cells by isorhamnetin and chloroquine. *J Exp Clin Cancer Res* 2019; 38: 225.
47. Wagner S, Ruff HM, Weber SL, et al. Reactive oxygen species-activated Ca/calmodulin kinase IIdelta is required for late I(Na) augmentation leading to cellular Na and Ca overload. *Circul Res* 2011; 108: 555–565.

48. Anderson ME. Oxidant stress promotes disease by activating CaMKII. *J Mol Cell Cardiol* 2015; 89: 160–167.
49. Chang H, Sheng JJ, Zhang L, et al. ROS-induced nuclear translocation of calpain-2 facilitates cardiomyocyte apoptosis in tail-suspended rats. *J Cell Biochem* 2015; 116: 2258–2269.
50. Sun P, Liu DZ, Jickling GC, et al. MicroRNA-based therapeutics in central nervous system injuries. *J Cereb Blood Flow Metab* 2018; 38: 1125–1148.
51. Keep RF, Andjelkovic AV, Xiang J, et al. Brain endothelial cell junctions after cerebral hemorrhage: changes, mechanisms and therapeutic targets. *J Cereb Blood Flow Metab* 2018; 38: 1255–1275.
52. Wilkinson DA, Keep RF, Hua Y, et al. Hematoma clearance as a therapeutic target in intracerebral hemorrhage: from macro to micro. *J Cereb Blood Flow Metab* 2018; 38: 741–745.